

I.Yu. Silachyov^{1*} , V.A. Glagolev² ¹Institute of Nuclear Physics, Almaty, Kazakhstan²Institute of Geological Sciences named after K.I. Satpayev, Almaty, Kazakhstan

*e-mail: silachyov@inp.kz

(Received 16 October 2021; received in revised form 19 May 2022; accepted 25 May 2022)

Comparator neutron activation analysis of the solid volumetric rock samples for gold content

Abstract. The application of comparator instrumental neutron activation analysis (INAA) combined with the internal standard method was considered to analyze solid volumetric samples of different rocks, 15–20 g of the mass, for Au content. Fe was used as the internal comparator with its mass fraction determined by X-ray fluorescence method (XRF) with the help of a laboratory energy dispersive XRF spectrometer RLP-21T, Kazakhstan. The puck-like samples about 29 mm across diameter and about 10 mm of the thickness were sliced up from rock drill-cores with a diamond saw. No other pretreatment was applied. Sample dimensions were fitted in compliance with that of the XRF spectrometer dishes to substitute them during analysis, i.e. they were the highest possible allowed by the spectrometer. Relative corrections for neutron self-shielding and for gamma-ray self-absorption by the samples of the same dimensions corresponding by their macrocomponent composition to the different types of common rocks turned out rather small, simply accounted using the internal standard, and almost irrespective of the rock types. By the example of serpentinite, picrite and diabase-picrite samples (Western Ulytau Belt, Central Kazakhstan) the whole approach was found as rather expedite and reliable being applied to determine Au content of sufficiently homogeneous magmatic and metamorphic rocks. More efforts resulting in Fe multiple measurements due to its heterogeneous distribution are necessary to analyze industrially significant Au contents in sedimentary rocks like black shales (Bakyrchik, Eastern Kazakhstan).

Key words: Neutron activation analysis, internal standard, gold, volumetric samples.

Introduction

Various analytical methods of rock investigation for gold content are known in multitudes [1-3]. Most of them include decomposition of the powdered samples followed by a separation and concentration technique and a highly sensitive instrumental determination. Intensive chemical pretreatment is the main drawback of the methods since it is often laborious and expensive, depends on reagent blank, and doesn't prevent loss of analyte and/or solution contamination. Overall Au content can be significantly underestimated if gold is locked-in or encapsulated in silicates or in a refractory (sulphide) matrix [1, 4].

Sample preparation for chemical digestion presents a separate problem. Gold mainly occurs in the rocks as native grains extremely variable in size and as diverse compounds incorporated in the common sulphide minerals [5]. Due to the substantially different density of the ground particles gravitational separation easily occurs, hence

homogeneous analytical subsamples can be hardly picked. To minimize this and the inherent “nugget effect”, the sample mass should be increased to 10 g and even more [6]. Moreover, soft and malleable gold grains are highly resistant to grinding. The grains may adhere to the walls of milling vessels causing losses of gold from some samples [3, 5] and contaminating the others.

The most dependable way of overcoming these difficulties is to exclude sample grinding and chemical pretreatment (i.e. to apply an initially instrumental method) and to use larger assays for analysis. Few analytical techniques can meet these requirements taking account of the sensitivity of gold determination close to ppb level necessary in geochemical explorations.

Rapidly developing laser ablation inductively coupled plasma mass spectrometry (LA-ICP-MS) having become a highly demanded way of Au local determination in the gold-bearing minerals [7-9] could be such a technique. Heterogeneity of laser-ablation target is tided over by using fused samples

prepared by the same way as for X-ray fluorescence (XRF) [10-11] and this makes possible to implement bulk analysis [12]. The studied rocks are completely turned into borate glasses including refractory minerals. Sample contamination with flux or crucible material is not crucial in case of Au determination, but limit of detection (LOD) is increased due to dilution. However, the uncertainty resulting from initial geological sample grinding still persists since only the powdered rock material is fused in an oven.

High energy instrumental photon activation analysis (IPAA) based on the photoexcitation reaction $^{197}\text{Au}(\gamma, \gamma')^{197\text{m}}\text{Au}$ is the best suited to analyze large, up to 0.5 kg of the mass, samples with gold inhomogeneous distribution [13]. A rather short half-life $T_{1/2}$ of $^{197\text{m}}\text{Au}$ isomer (7.3 s) is considered as its only inconvenience¹. IPAA soundly found its broad application in gold mining but it can be scarcely employed in geochemistry due to insufficient LOD values reaching 0.1–0.2 ppm at the best (0.5–1.0 ppm most commonly) using a semiconductor detector [14].

Apart from 14 MeV instrumental neutron activation analysis (INAA) which doesn't compete in sensitivity with INAA by thermal neutrons [15] the latter seems being the most appropriate for gold geochemical survey owing to its extremely low LOD value in rocks up to 2 ppb [3]. Individual sample mass varies over a very wide range – from ≈ 100 mg [8, 16] to several hundreds of g and more to reduce severe heterogeneity [3, 17]. If it exceeds 0.5–1.0 g, a sample can no longer be considered as «a point source», and neutron self-shielding, neutron-flux gradients in the sample and self-absorption of gamma rays must be accounted [18]. Without discussing different ways to overcome these difficulties, internal standard based INAA applying in-situ relative detection efficiency should be mentioned since it takes care of the neutron flux perturbation inside the samples [19]. A suitable reference element determined by a convenient analytical technique is used as the internal standard. The method found its broad application to analyze large heterogeneous samples including industrial dross for noble elements [20].

In the present work comparator INAA was tried to determine Au content of solid samples – plane cylindrical pieces of the drill cores, 15–20 g of the mass, cut from several types of common rocks. Minimum nondestructive pretreatment excluded any losses of gold or sample contamination. Iron was chosen as the internal standard with its mass fraction

found by XRF as in some previous investigations of rock element composition [21-23].

Materials and methods

Total content of the natural gold including its nanoforms (“invisible gold”) was studied in picrites, diabase-picrites, and serpentinites picked in the Karatugay Complex of the Western Ulytau Belt (Central Kazakhstan) with a view of searching new ore occurrence of the non-ferrous and noble metals. The drill-core samples 28.5–29.0 mm across diameter were cut with a diamond saw into planar cylinders 9.5–10.0 mm of the thickness. This was the end of the whole preparation. The obtained analytical samples came in smooth enough, without visible roughness of the flat surfaces; small lateral chips of the hard rock, if any, were ignored. An exterior view of several similar analytical samples is presented in Fig. 1.

The sample sizes were determined by the dimensions of the measuring chamber of an energy dispersive XRF spectrometer RLP-21T used in the investigation. The rock samples were installed instead of the steel dishes for powdered specimens inside the sample changer. Their diameter corresponded to the external diameter of the dishes, and the height depended on the gap between the cover and the collimator. So, the sample sizes were close to the maximum one for the given equipment. Fig. 2 demonstrates the charged sample changer of the spectrometer.

RLP-21T was designed and produced by LLP “AspapGeo” (Almaty, Kazakhstan) to study element composition of rocks, minerals, ores, and concentrates. The accuracy of its software was repeatedly confirmed with the help of different corresponding certified reference materials (CRMs). The ascribed uncertainty of iron content measuring in rock samples is 2–8%. RLP-21T is enrolled in the State Register of Measuring Devices (Certificate № 670, valid to 27.07.2025), and the corresponding analytical technique is registered by the National Body for Certification of Kazakhstan (Certificate № 69-2022, valid to 15.02.2027).

To implement INAA each puck-like sample was sealed in polyethylene and then wrapped in aluminium foil. Several samples (no more than six at once) were stacked up and fixed in the same wrapping. Taking account of their dimensions, the packages were placed upright in the irradiation container to be oriented along the channel axis. Samples layout in the irradiation channel is presented in Fig. 3. In this case the flats of the cylindrical samples were

¹ The more convenient $^{197}\text{Au}(\gamma, n)^{196}\text{Au}$ reaction ($T_{1/2} = 6.2$ d) results in lower sensitivity.

lined parallel to the radial component of the neutron flux gradient (about 9% per 1 cm). This is the least favorable orientation if the gradient were considered either empirically or theoretically. However, it didn't matter in the present investigation since the neutron flux gradient was accounted automatically by using the internal standard method.



Figure 1 – Sliced up samples of serpentinite drill-core prepared for the investigation



Figure 2 – RLP-21T with open lid and charged sample changer

All the packages were irradiated one by one for 1 min including the transportation time in the position №4 inside the peripheral vertical channel №10-6 of the light-water research reactor WWR-K (Almaty) by the thermal neutron flux density $8.9 \times 10^{13} \text{ cm}^{-2} \text{ s}^{-1}$; the fast neutron flux density amounted to $6.0 \times 10^{12} \text{ cm}^{-2} \text{ s}^{-1}$ [24]. The first package included a zirconium monitor of the neutron flux – 10 mg of ZrO_2 (the Institute of Reference Materials, Ekaterinburg, Russian Federation) sealed in small thin double polyethylene bag placed in the middle. Due to the short-timed irradiation, the neutron flux parameters were considered invariable.

Gamma-spectrometric measurements of the studied samples were conducted after 9–10 days of decay when radionuclide ^{24}Na mainly in charge of the background rise due to the Compton continuum practically completely decayed. Counting time was about 40 min and the distance from the detector cap to the bottom of the volumetric samples was 19 mm or 24 mm to their centers.

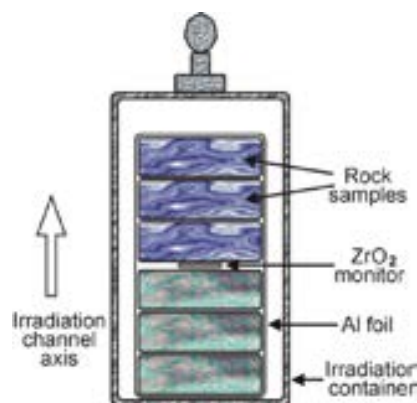


Figure 3 – Samples layout in the irradiation channel

All the measurements were performed using an extended-range HPGe detector GX5019 with a relative efficiency of 50% and an energy resolution of 1.86 keV at the 1332 keV peak of ^{60}Co , connected to a Canberra multi-channel analyzer DSA-1000. Detector calibration for relative detection efficiency was made with the help of a multi-gamma ray standard MGS-1 (^{152}Eu , ^{154}Eu , ^{155}Eu) and an isotopic source ^{133}Ba , both by Canberra. A fourth power polynomial was used for the fitting of calibration curve. Spectra collection and subsequent treatment were carried out by the “AnalGamma” software developed in the Institute of Nuclear Physics to provide gamma-ray spectrometric analysis. The software approximates a part of gamma-ray spectrum in the treatment window by Gaussian curves and a flat background and calculates peak count rates in cps. Partly overlapping peaks can be reliably resolved. Quality of the approximation is checked by the X^2 test.

Gold content of the samples was determined by the only intensive gamma-line of the radionuclide ^{198}Au with the energy E equals to 411.80 keV and quantum yield P_γ reaching 95.6%. Actually there are no unresolved spectral interferences to this gamma-line when different rocks are analyzed with the exception of the low-intensive line of ^{152}Eu ($E = 411.12 \text{ keV}$, $P_\gamma = 2.2\%$) which should be accounted if gold mass fractions get close to the LOD values for these objects.

Results and discussion

Au as well as other element contents of the samples C_a (%) can be calculated according to the next equation of simple comparator method of standardization in INAA [25] using the internal standard method [26] (lower case indices a and c mean an analyzed element and the comparator, respectively):

$$C_a = C_c \frac{k_{0,c} J_a \varepsilon(E_c) (f + Q_0^c) (SD)_c G_c F_c}{k_{0,a} J_c \varepsilon(E_a) (f + Q_0^a) (SD)_a G_a F_a} K_{a,c} \quad (1)$$

where C_c is the element comparator content of the sample (%), k_0 is k_0 -factor relatively to 411.8 keV gamma-line of radionuclide ^{198}Au for the gamma-lines of the comparator and an analyzed element [27], J is the full-energy peak count rate of the corresponding radionuclide analytical gamma-ray (cps), $\varepsilon(E)$ is the relative detection efficiency of the measured gamma-line (%), Q_0 is the resonance integral I_0 (cm^2) to the thermal neutron cross-section σ_0 (cm^2) ratio, f is the thermal to epithermal neutron flux ratio, $S = 1 - \exp(-\lambda t_{irr})$ is saturation factor, $D = \exp(-\lambda t_d)$ is decay factor (t_{irr} and t_d are irradiation and decay time), G is the correction factor for neutron self-shielding by the sample, F is the correction factor for analytical gamma-ray self-absorption by the sample.

When INAA of rock samples for the long-lived radionuclides is carried out correction for the measuring time is always <1% and can be neglected.

The empirical correction factor $K_{a,c}$ is applied to compensate for an analytical bias caused by the errors of detector calibration for detection efficiency, absence of Q_0 correction for the deviation of thermal neutron flux from $1/E$ law, and by other reasons. In particular, using the same counting geometries, there is no need to correct J for true coincidences. In case of gold analysis $K_{a,c}$ value was determined with the help of a European Commission CRM IRMM-530R (Al-0.1% Au alloy) and an assay of chemically pure (reduced) iron. Then it was verified using some multi-element CRMs certified for gold contents (see below).

The model ratio $1/f$ was evaluated by the “bare bi-isotopic method” with the help of a ZrO_2 monitor of the neutron flux spectral composition. The corresponding expression was adduced more than once in the previous investigations [21-23]. As for the present work, $1/f$ value amounted to 0.0330 ± 0.012 ($P = 0.95$).

To assess thermal and resonance neutron self-shielding by the analyzed puck-like samples, a

similar model one, i.e. 29 mm across diameter and 10 mm of the thickness, was considered corresponding by its composition to the average content of the main rock-forming oxides of the continental crust [28]. Mass fractions of Sm, Eu and Gd characterized by the maximum values of σ_0 were taken equal to their average crustal abundance (Clarke numbers) [29]. With the density equal to 2.8 g cm^{-3} close to the rocks mean value the model sample mass reached 18.5 g.

The effective neutron self-shielding factors for gold $G_{eff, Au}$ and iron $G_{eff, Fe}$ were evaluated with the help of the spreadsheet by C.Chilian, et al. [30] kindly granted by the authors. The model values are presented in Table 1. Both factors appeared close to a unit and differ by no more than 1% one from another. The latter confirms that conducting INAA for Au content, Fe as the internal standard can effectively take account of the neutron self-shielding by the model rock sample.

To verify this conclusion for broader cases which take place in geochemical investigations the same assessment was made for a range of magmatic rocks differing by their silica content – from felsic to ultramafic ones. Typical macrocomponent composition of the rocks was picked up from the CRM catalogues (Russian Federation). $G_{eff, Au}$ and $G_{eff, Fe}$ factors for different rocks appeared very close to that for the continental crust (Table 1) with their ratio practically a constant.

If Sm, Eu, and Gd contents of the model rock sample are increased by one order of magnitude, coefficients $G_{eff, Au}$ and $G_{eff, Fe}$ decrease to 0.946 and 0.919 correspondingly, and their ratio differs from a unit by no more than 3%. It's interesting to note that in this case, including even higher contents of the rare earths, another element such as Rb, Cs, As, Ba, Sm, or Th characterized by high values of Q_0 can take account of thermal and resonance neutrons self-shielding more correctly with their mass fractions being determined by an independent method [31].

Finally, $G_{eff, Au}$ and $G_{eff, Fe}$ values very slightly depend on rock density and their ratio remains a constant.

Correction for analytical gamma-ray self-absorption was estimated according to the equation providing its simplified description in cylindrical samples [32]:

$$\frac{F_c}{F_a} = \frac{\mu(E_a)(1 - \exp(-\rho\mu(E_c)h))}{\mu(E_c)(1 - \exp(-\rho\mu(E_a)h))} \quad (2)$$

where $\mu(E)$ is photon mass attenuation coefficient ($\text{cm}^2 \text{ g}^{-1}$); ρ – sample density (g cm^{-3}) and h

– sample thickness (cm). $\mu(E)$ values of ^{198}Au and ^{59}Fe analytical gamma-lines in the chemical compounds corresponding to the main rock-forming oxides were picked up from an NIST database [33] and presented in Table 2. It takes note, that due to the high enough energy of these radionuclides gamma-lines, $\mu(E)$ values are quite close for different compounds since interaction of gamma-rays with the matter in this case is mainly brought to the

scattering processes. Hence the corresponding total mass attenuation coefficients $\mu_{\Sigma}(E)$ are practically independent of the rock composition (Table 1). The same is correct for F factors too, and their ratio is practically a constant for different types of magmatic rocks: $F_{\text{Fe}}/F_{\text{Au}} = 1.045$. According to Eq. 2, this ratio very slightly linearly depends on the rock density; it changes by no more than 1% if ρ varies within 2.3–3.2.

Table 1 – Composition of the continental crust and different magmatic rocks (wt.%,) their total photon mass attenuation coefficients of ^{198}Au and ^{59}Fe analytical gamma-lines, and the corresponding self-absorption and neutron self-shielding coefficients for the puck-like solid samples

	Continental crust [28]	Felsic rocks		Intermediate rocks		Mafic rocks		Ultramafic rocks	
		Granite (SG-3)	Granodiorite (MK-2)	Quartz diorite (SKD-1)	Synnyrite (SSN-1)	Anorthosite (MO-6)	Gabbro (SGD-2A)	Dunite (SDU-1)	Hornblendite (MU-3)
SiO_2	59.1	74.8	64.5	60.5	55.0	51.8	46.6	39.6	37.9
Al_2O_3	15.8	10.6	16.6	16.6	22.5	22.8	14.9	0.97	14.2
Na_2O	3.2	4.24	4.27	3.57	1.19	4.04	2.72	0.035	2.14
K_2O	1.88	4.64	3.12	2.98	18.0	0.76	3.09	0.010	0.382
MgO	4.4	0.10	1.58	3.05	0.18	2.10	6.81	41.9	12.7
CaO	6.4	0.32	3.83	4.84	0.49	10.1	10.68	1.52	11.0
TiO_2	0.7	0.26	0.63	0.86	0.091	1.87	1.72	0.018	1.91
MnO	0.11	0.12	0.083	0.086	0.0093	0.076	0.167	0.13	0.144
Fe_2O_3	6.6 ^a	4.50	4.64	5.55	1.35	6.26	11.3	8.91	18.3
P_2O_5	0.2	0.024	0.229	0.17	0.058	0.140	1.03	0.010	0.032
SO_3	-	-	0.020	0.033	0.0625	0.173	0.038	0.103	0.135
CO_2	-	-	0.10	0.18	-	0.36	-	1.61	0.13
$G_{\text{eff, Au}}$	0.982	0.981	0.982	0.982	0.973	0.982	0.979	0.985	0.977
$G_{\text{eff, Fe}}$	0.973	0.972	0.973	0.973	0.960	0.974	0.968	0.978	0.966
$\mu_{\Sigma}(412 \text{ keV}), \text{cm}^2 \text{g}^{-1}$	0.0927	0.0939	0.0938	0.0926	0.0931	0.0945	0.0934	0.0893	0.0932
$\mu_{\Sigma}(1099 \text{ keV}), \text{cm}^2 \text{g}^{-1}$	0.0593	0.0601	0.0600	0.0593	0.0596	0.0604	0.0596	0.0571	0.0594
F_{Au}	0.881	0.879	0.879	0.881	0.880	0.879	0.880	0.885	0.880
F_{Fe}	0.921	0.920	0.921	0.921	0.921	0.920	0.921	0.924	0.921

^a – FeO

Table 2 – Coefficients of photon mass attenuation of ^{198}Au and ^{59}Fe analytical gamma-lines by the Earth crust rock-forming oxides

Rock-forming oxide	$\mu(412 \text{ keV}), \text{ cm}^2 \text{ g}^{-1}$	$\mu(1099 \text{ keV}), \text{ cm}^2 \text{ g}^{-1}$
SiO_2	0.0947	0.0608
Al_2O_3	0.0930	0.0597
Na_2O	0.0917	0.0588
K_2O	0.0939	0.0596
MgO	0.0941	0.0604
CaO	0.0960	0.0609
TiO_2	0.0916	0.0580
MnO	0.0910	0.0569
Fe_2O_3	0.0932	0.0579
P_2O_5	0.0936	0.0600
SO_3	0.0949	0.0608
CO_2	0.0945	0.0608

So, the effects of neutron self-shielding by the regularly-shaped samples of common rocks like represented in Fig. 1, and of gamma-ray self-

absorption, are not too significant and are simply corrected if needed. Therefore accuracy of gold determination by comparator INAA using Eq. 1 can be verified with the help of usual powered CRMs certified for Au content.

To minimize the influence of gold heterogeneous distribution in the CRMs produced from gold-bearing ores, recommended sample mass of the latter taken for an analysis must be not less than 5 g. Such a wasteful expenditure of the CRMs was avoided by selecting the ones prepared from the homogeneous products of ores chemical processing – flotation concentrates and similar (Table 3). All these CRMs are produced in Russian Federation: the first two by the Scientific-Research and Design Institute of Non-Ferrous Metallurgy (Krasnoyarsk), the others by the Vinogradov Institute of Geochemistry (Irkutsk). About 100 mg of the CRMs were sealed in plain double polyethylene bags and irradiated for 1 h. Their masses corresponded to the minimum ones recommended by the producers to guarantee gold homogeneous distribution. The samples were counted using the same gamma-ray spectrometer after 10–12 d of decay at the distance of 24 mm from the detector cap.

Table 3 – Gold content of the powered CRMs by comparator INAA using iron as the internal standard ($P = 0.95$)

CRM name	CRM type	Fe, %	Au, mg kg $^{-1}$		E_n -number
			Certified value	Measured value	
SHT-1	Matte of ore thermal melt	49.43 ± 0.67	1.62 ± 0.16	1.57 ± 0.15	-0.23
FSHT-42	Copper-nickel nis matte	2.64 ± 0.17	2.55 ± 0.11	2.60 ± 0.25	0.18
GSO 1787	Flotation concentrate	29.45 ± 0.50	36 ± 1	36.0 ± 3.0	0
GSO 1788	Flotation concentrate	26.97 ± 0.50	33 ± 1	32.4 ± 3.0	-0.19
GSO 2739	Flotation concentrate	28.44 ± 0.50	34 ± 1	34.3 ± 3.0	0.09
GSO 2740	Flotation tailings	4.24 ± 0.17	0.9 ± 0.1	0.94 ± 0.09	0.30

The first two CRMs in Table 3 are characterized by maximum total contents of medium-heavy elements (Fe, Ni, Cu, Se) amounting to 71% and 78%, correspondingly. Nevertheless, due to high values of ^{198}Au and ^{59}Fe analytical gamma-lines and small bag thickness (≈ 1 mm) relative correction for gamma-ray self-absorption evaluated by Eq. 2 is lower than 1% and can be neglected.

Expanded uncertainty of the INAA results $U(C_a)$ was estimated as follows ($P = 0.95$):

$$U(C_a) \approx 2C_a \sqrt{\frac{u(J_a)^2}{J_a^2} + \frac{u(J_c)^2}{J_c^2} + \frac{u(C_c)^2}{C_c^2} + \delta_a^2}, \quad (3)$$

Int. j. biol. chem. (Online)

where $u(J_a)$, $u(J_c)$, and $u(C_c)$ are standard uncertainties of the corresponding values as in Eq. 1, δ_a is the standard deviation of gold determination (methodical uncertainty) by comparator INAA (all the ratios and δ_a are in %). The last value assessed earlier with the help of the CRMs equals $\approx 3\%$. Standard uncertainty of iron internal comparator content of a sample by XRF corresponded to the ascribed values according to the certified analytical technique.

The results of CRM analyses for gold mass fraction by comparator INAA using Eq. 1 ($P = 0.95$) are presented in Table 3. Iron content of the samples was determined by XRF. The measured values are

well comparable with the certified ones with <5% of discrepancy. Expanded uncertainty of all the six CRM analyses by comparator INAA doesn't exceed the allowable standard deviation of the results of their determination directed by the III category of precision (of analysis) (5.4–27% for the intervals including these contents) according to OST 41-08-221-04 [34]².

On the other hand, E_n -number usually used as a recommended by IUPAC criterion to verify laboratory performance [35] also showed good agreement between all certified and measured values within acceptable value ± 1 .

The results of Au determination in volumetric samples of several types of rocks by comparator INAA are presented in Tables 4–7 together with their values of mass and density. To assess heterogeneity of Fe content of the samples used as the internal standard they were measured twice changing the sides faced to the collimator of RLP-21T. During gamma-ray counting to find Au mass fraction, the samples were accordingly turned over as well.

Fe content of the first four serpentinite samples (Table 4) differs up to 10% depending on the side faced to the collimator. However, Fe was found to be distributed more homogeneously within each flat surface of the samples. Rotating each sample around its axis, Fe mass fraction varied by less than 5%. Au mass fraction of the serpentinite samples doesn't exceed its four limits of detection evaluated according to the next expression commonly applied in spectroscopic methods: $LOD = 3.3\sigma_b/b$ [36]. Here σ_b is standard deviation of the blank signal (counting statistics of the background count rate at the peak area) and b is concentration sensitivity of the method. If a linear calibration function is used like in INAA, b is a constant: $b = \Delta J / \Delta C$. The limit of Au detection reached very low value <0.001 $\mu\text{g g}^{-1}$ in the serpentinite samples since this ultramafic rock is characterized by negligible content of Sc ($\approx 3 \mu\text{g g}^{-1}$) which corresponding radionuclide is often mainly in charge of the Compton continuum under ^{198}Au analytical gamma-line after ^{24}Na completely decayed.

The next three Tables (5–7) present rather homogeneous distribution of iron in the rock samples, especially in picrites. Au content of all diabase-picrites is lower the LOD value for these samples which turned out four times as high comparing with that of serpentinite samples. This is caused by

² For the samples with fine-dispersed gold <0.1 mm of the size.

high Sc mass fraction reaching its threefold Clarke number ($\approx 65 \mu\text{g g}^{-1}$) and higher Fe content comparing with serpentinites. Maximum content of Au in picrite samples doesn't exceed $\approx 0.01 \mu\text{g g}^{-1}$ that is five times as high as the corresponding LOD value ($C_{sc} \approx 18 \mu\text{g g}^{-1}$).

On the whole Au mass fraction in the several types of common magmatic and metamorphic rocks was found close to its Clarke number [29]. Fe is fairly homogeneously distributed, so only two measurements are sufficient to evaluate its content of the sample, i.e. to analyze Au reliably.

Solid volumetric samples of rocks being used in INAA can't offer an advantage of the sensitivity improvement comparing with the small powdered ones. However, they permit to avoid the sample preparation difficulties mentioned above, particularly representative sub-sampling [37], and therefore can be preferable in geochemical investigations of gold behavior. In any case, the gained limit of Au detection is quite enough for this purpose.

The volumetric sample advantages become of the distinctive excellence when the industrially significant Au contents are concerned. One of such potentially promising source of gold is associated with a sedimentary rock – black shales [38] widely spread in the upper crust. Three corresponding puck-like samples like the ones above were prepared from the large pieces of rock picked in the gold deposit Bakyrchik, Eastern Kazakhstan. 29 mm across the diameter, they differed in their thickness (7.5 or 10 mm) and hence in mass. XRF showed considerable As content of the samples about 3%, hence gold can be associated with the mineral fraction including arsenopyrite.

Unlike the samples of magmatic and metamorphic rocks investigated above, that of the black shales revealed high heterogeneity of Fe mass fraction by XRF. Each side of a sample was measured four times being rotated by 90° around its axis. The values of relative standard deviation of these measurements are presented in Table 8.

Such contradictory results of separate determination of iron content in the heterogeneous sedimentary rock samples are obviously caused by very low maximum penetration depth d (cm) of Fe characteristic X-rays. According to “the 1% approximation” (i.e. 99% of the X-rays with the certain energy are completely absorbed by the medium), this value was evaluated as follows [39] taking account of approximate macrocomponent content of the samples:

Table 4 – Iron and gold content of the serpentinite samples ($P = 0.95$), site Akzhal

Sample name	Sample mass, g	Sample density, g cm ⁻³	Fe, %		Au, µg g ⁻¹	
			First side	Reverse side	First side	Reverse side
Akzhal 7/1	14.19	2.23	4.64 ± 0.17	4.22 ± 0.17	<0.001	<0.001
Akzhal 7/2	14.20	2.27	4.83 ± 0.17	5.35 ± 0.30	<0.001	<0.001
Akzhal 7/3	13.43	2.26	4.97 ± 0.17	4.85 ± 0.17	0.0040 ± 0.0006	0.0045 ± 0.0006
Akzhal 7/4	14.22	2.30	5.05 ± 0.30	4.57 ± 0.17	<0.001	<0.001
Akzhal 7/5	14.03	2.23	4.50 ± 0.17	4.78 ± 0.17	0.0015 ± 0.0005	0.0016 ± 0.0005
Akzhal 7/6	14.52	2.31	5.28 ± 0.30	5.02 ± 0.30	0.0021 ± 0.0005	0.0015 ± 0.0005

Table 5 – Iron and gold content of the diabase-picrite samples ($P = 0.95$), site Akzhal

Sample name	Sample mass, g	Sample density, g cm ⁻³	Fe, %		Au, µg g ⁻¹	
			First side	Reverse side	First side	Reverse side
Akzhal 8/1	19.18	3.17	14.43 ± 0.45	13.98 ± 0.45	<0.004	<0.004
Akzhal 8/2	18.87	3.12	14.11 ± 0.45	13.61 ± 0.45	<0.004	<0.004
Akzhal 8/3	18.87	3.12	13.70 ± 0.45	14.06 ± 0.45	<0.004	<0.004
Akzhal 8/4	18.41	3.04	14.18 ± 0.45	14.38 ± 0.45	<0.004	<0.004
Akzhal 8/5	17.05	2.92	13.15 ± 0.45	14.23 ± 0.45	<0.004	<0.004

Table 6 – Iron and gold content of the picrite samples ($P = 0.95$), site Karatugay

Sample name	Sample mass, g	Sample density, g cm ⁻³	Fe, %		Au, µg g ⁻¹	
			First side	Reverse side	First side	Reverse side
Karat 12/1	18.76	2.99	9.24 ± 0.30	9.20 ± 0.30	<0.002	<0.002
Karat 12/2	17.64	2.91	9.30 ± 0.30	9.66 ± 0.30	0.011 ± 0.002	0.010 ± 0.002
Karat 12/3	18.26	2.90	9.30 ± 0.30	9.31 ± 0.30	<0.002	<0.002
Karat 12/4	18.44	2.93	9.24 ± 0.30	9.41 ± 0.30	<0.002	<0.002
Karat 12/5	18.35	3.03	9.16 ± 0.30	8.92 ± 0.30	0.006 ± 0.002	0.006 ± 0.002

Table 7 – Iron and gold content of the picrite samples ($P = 0.95$), site Karatugay

Sample name	Sample mass, g	Sample density, g cm ⁻³	Fe, %		Au, µg g ⁻¹	
			First side	Reverse side	First side	Reverse side
Karat 13/1	16.67	2.66	9.10 ± 0.30	9.46 ± 0.30	<0.002	<0.002
Karat 13/2	16.94	2.70	8.92 ± 0.30	8.80 ± 0.30	<0.002	<0.002
Karat 13/3	16.79	2.68	9.03 ± 0.30	8.88 ± 0.30	<0.002	<0.002
Karat 13/4	17.68	2.82	9.05 ± 0.30	8.97 ± 0.30	<0.002	<0.002
Karat 13/5	18.05	2.88	8.89 ± 0.30	8.90 ± 0.30	<0.002	<0.002

$$d = \frac{4.61}{\rho(\mu_i(E_i)/\sin\varphi_i + \mu_x(E_x)/\sin\varphi_x)}, \quad (4)$$

where indices i and x mean the primary and characteristic X-rays, respectively, φ_i and φ_x are the incidence and take-off angles. The calculated r value of the black shale samples was about 3.3 g cm^{-3} . Then taking φ_i and φ_x both close to 45° , $E_x = 6.4 \text{ keV}$ (Fe K -alpha line) and $E_i = 23.2 \text{ keV}$ (K -alpha line of Cd intermediate target) the penetration depth of Fe characteristic X-rays amounted $\approx 0.15 \text{ mm}$ only. Though that of As characterized by more high-energy X-ray lines reached $\approx 0.30 \text{ mm}$, As was rejected as the internal standard since its distribution turned out even more heterogeneous (Table 8).

Thus, to evaluate Au content of the black shale volumetric samples the mean values of eight Fe measuring by XRF were used (Table 9). The presented Fe mass fractions are averaged over four measurements of each side.

Because of As high content the irradiated samplers were counted after three weeks of decay when ^{76}As count rate became acceptable. In accordance with

the model realized in the spreadsheet, $G_{\text{eff, Fe}}$ to $G_{\text{eff, Au}}$ ratio for the black shale samples (Eq. 1) equaled 0.985 irrespective of their different thickness and As mass fraction. Correspondingly $F_{\text{Fe}}/F_{\text{Au}}$ ratio amounted to 1.056 for the thicker sample and to 1.042 for the other two (Eq. 2). Then taking these corrections Au contents were calculated (Table 9). They were found very close turning over the samples during counting. This can seemingly witness to the homogeneous distribution of gold in the samples (along the axes at least) i.e. to its preferable presence as the invisible nanoforms.

Table 8 – Relative standard deviation (%) of iron and arsenic determination in the black shale samples ($n = 4$), gold deposit Bakyrchik

Sample name	Fe		As	
	First side	Reverse side	First side	Reverse side
ZHB 4/1	20.8	12.4	18.5	12.7
ZHB 4/2	9.0	6.9	11.8	10.0
ZHB 4/3	4.1	7.0	5.9	12.2

Table 9 – Iron and gold content of the black shale samples ($P = 0.95$)

Sample name	Sample mass, g	Sample density, g cm^{-3}	Fe, %		Au, $\mu\text{g g}^{-1}$	
			First side	Reverse side	First side	Reverse side
ZHB 4/1	15.82	3.26	11.31 ± 0.45	13.18 ± 0.45	3.66 ± 0.36	3.60 ± 0.36
ZHB 4/2	21.63	3.30	13.33 ± 0.45	16.19 ± 0.45	4.43 ± 0.44	4.48 ± 0.44
ZHB 4/3	16.24	3.28	16.48 ± 0.45	15.46 ± 0.45	5.15 ± 0.53	5.18 ± 0.50

According to the peculiarities of gold behavior during sample preparation mentioned in Introduction, correctness of Au determination in volumetric samples by comparator INAA can be hardly confirmed by other analytical techniques. In this case accuracy of the results is ensured by the following:

- total absence of any sample preparation including grinding;
- verification of the accuracy of detector calibration and concentration standardization with the help of high-quality powered CRMs certified for Au content;
- application of the internal standard method allowing to minimize all main corrections making them practically independent of the sample composition and therefore almost negligible;

- reliable determination of the internal standard content of the samples by an independent method.

The last condition depends not on the method itself but on the samples too, i.e. on their intrinsic heterogeneity, and is seemingly discussable. Different instrumental methods and different internal standards can be tried. At last, a part of the samples can be crushed and powdered after INAA measurements are completed to find internal comparator content in case of its high heterogeneity. In any case, this doesn't deny the whole approach.

Conclusion

An internal standard based variant of comparator INAA was tried to determine Au content of solid volumetric samples of several

types of the widely spread rocks. Fe content of the samples as the internal comparator was determined by XRF. No pretreatment of the geological material was applied. Shape and dimensions of the samples cut as plane cylindrical pieces of the drill cores corresponded that of the dishes being used to implement elemental analysis with the help of an energy dispersive XRF spectrometer RLP-21T. Significantly enlarged sample mass to 15–20 g makes possible to take account of gold distribution heterogeneity to a great extent, if any. Application of Fe as the internal standard allowed essentially reducing corrections for neutron self-shielding and for gamma-ray self-absorption by the volumetric samples to the values no more than 1% and 5%, correspondingly. The corrections were shown to be practically irrespective of major constituents of different types of rocks.

High penetrability of neutrons and high-energy gamma-rays being taken into account, when the corresponding analytical signals of ^{198}Au and ^{59}Au are formed by the whole sample volume, reliability of gold determination depends on the correctness of iron analysis by XRF. The demonstrated simple high-sensitive approach can be considered as a rather convenient and reliable one in case of geochemical exploration of homogenous rocks, when low penetration depth of Fe characteristic X-rays (<1 mm) doesn't matter. XRF should be gingerly applied to determine Fe if sedimentary and other rocks characterized by its significant heterogeneity are analyzed for industrially significant Au contents. Other macroelements surely determined both by INAA and XRF may be tried then as the internal standards, or another method of Fe determination can be applied.

Acknowledgments

The work was supported by the grants BR09158958 from Ministry of Education and Sciences of the Republic of Kazakhstan and BR10264324 from Committee of Geology, Ministry of Ecology, Geology, and Mineral Resources of the Republic of Kazakhstan.

References

- Balaram V. (2008) Analytical methods for gold and other precious metals in exploration studies. *J Appl Geochem*, vol. 10(2A), pp. 545-562.
- IAEA-TECDOC-1443 (2005) Nuclear analytical methods for platinum group elements. Vienna: IAEA, 53 p. ISBN 92-0-102405-3.
- Hoffman E.L., Clark J.R., Yeager J.R. (1998) Gold analysis – fire assaying and alternative methods. *Explor Min Geol*, vol. 7, pp. 155-160.
- Helmecci W., Helmecci E., Baker L.A., et al. (2018) Development of a general acid method for the digestion of gold ore samples together with a comparison of extraction solvents for gold and determination by microwave-induced plasmaatomic emission spectrometry (MIP-AES). *J Anal At Spectrom*, vol. 33, pp. 1336-1344. <https://doi.org/10.1039/c8ja00136g>.
- Kontas E. (1993) Analytical methods for determining gold in geological samples. Report of investigation, Geological survey of Finland. Espoo, 43 p, ISBN 951-690-476-9.
- Liu Y.H., Wan B., Xue D.S. (2019) Sample digestion and combined preconcentration methods for the determination of ultra-low gold levels in rocks. *Molecules*, vol. 24, pp. 1778-1797. <https://doi.org/10.3390/molecules24091778>.
- Gao F., Du Y., Pang Zh., et al. (2019) LA-ICP-MS trace-element analysis of pyrite from the Huanxiangwa gold deposit, Xiong'ershan district, China: implications for ore genesis. *Minerals*, vol. 9(3), pp. 157-171. <https://doi.org/10.3390/min9030157>.
- Vikentyev I.V. (2015) Invisible and microscopic gold in pyrite: methods and new data for massive sulfide ores of the Urals. *Geol Ore Deposits*, vol. 57(4), pp. 237-265. <https://doi.org/10.1134/S1075701515040054>.
- Zhang J., Deng J., Chen H., et al. (2014) LA-ICP-MS trace element analysis of pyrite from the Chang'an gold deposit, Sanjiang region, China: implication for ore-forming process. *Gondwana Res*, vol. 26, pp. 557-575. <https://doi.org/10.1016/j.gr.2013.11.003>.
- Kil Y., Yung H. (2015) LA-ICP-MS analysis of natural rock samples using XRF glass beads. *Geosci J* (Seoul, Repub. Korea), vol. 19(1), pp. 45-52. <https://doi.org/10.1007/s12303-014-0063-1>.
- Tamura A., Akizawa N., Otsuka R., et al. (2015) Measurement of whole-rock trace-element composition by flux-free fused glass and LA-ICP-MS: evaluation of simple and rapid routine work. *Geochem J*, vol. 49, pp. 243-258. <https://doi.org/10.2343/geochemj.2.0353>.
- Stoll B., Jochum K.P., Herwig K., et al. (2008) An automated iridium-strip heater for LA-ICP-MS bulk analysis of geological samples. *Geostand Geoanal*, vol. 32(1), pp. 5-26. <https://doi.org/10.1111/j.1751-908X.2007.00871.x>.
- Segebade C., Starovoitova V.N., Borgwardt T., et al. (2016) Principles, methodologies, and

applications of photon activation analysis: a review. *J Radioanal Nucl Chem*, vol. 312(1), pp. 443-459. <https://doi.org/10.1007/s10967-017-5238-6>.

14. Řanda Z., Špaček B., Mizera J. (2006) Fast determination of gold in large mass samples of gold ores by photoexcitation reactions using 10 MeV bremsstrahlung. *J Radioanal Nucl Chem*, vol. 271(3), pp. 603-606. <https://doi.org/10.1007/s10967-007-0314-y>.

15. Nat A., Ene A., Lupu R. (2004) Rapid determination of gold in Romanian auriferous alluvial sands, concentrates and rocks by 14 MeV NAA. *J Radioanal Nucl Chem*, vol. 261(1), pp. 179-188. <https://doi.org/10.1023/B:JRNC.0000030954.29323.39>.

16. Ahmad K., Dampare S.B., Adomako D., et al. (2004) The use of neutron activation analysis in gold prospecting in small-scale mining in Ghana. *J Radioanal Nucl Chem*, vol. 260(3), pp. 653-658. <https://doi.org/10.1023/B:JRNC.0000028227.81455.f7>.

17. Yudakov A.A., Ivannikov S.I., Sheleznov V.V., et al. (2015) Neutron activation determination of gold in technogenic raw materials with different mineral composition. *Nucl Technol Radiat Prot*, vol. 30(4), pp. 273-279. <https://doi.org/10.2298/NTRP1504273Y>.

18. Menezes M.Â., Jaćimović R. (2014) Implementation of a methodology to analyse cylindrical 5-g sample by neutron activation technique, k_0 method, at CDTN/CNEN, Belo Horizonte, Brazil. *J Radioanal Nucl Chem*, vol. 300(2), pp. 523-531. <https://doi.org/10.1007/s10967-014-3074-5>.

19. Nair A.G.C., Acharya R., Sudarshan K., et al. (2003) Development of an internal monostandard instrumental neutron activation analysis method based on in situ detection efficiency for analysis of large and nonstandard geometry samples. *Anal Chem*, vol. 75(18), pp. 4868-4874. <https://doi.org/10.1021/ac034457d>.

20. Swain K.K., Ajith N., Acharya R., et al. (2012) Large sample neutron activation analysis of dross for gold and silver. *J Radioanal Nucl Chem*, vol. 294(2), pp. 319-322. <https://doi.org/10.1007/s10967-011-1519-7>.

21. Silachyov I.Yu. (2018) Determination of rare earths in uranium raw material by neutron activation analysis and X-ray fluorescence. *News of the Academy of Sciences of RK, ser. chem. & technol.*, vol. 429(3), pp. 28-38.

22. Silachyov I.Yu. (2020) Instrumental neutron activation analysis of rhenium in uranium raw material. *IJBC*, vol. 13(1), pp. 161-169. <https://doi.org/10.26577/ijbch.2020.v13.i1.17>.

23. Silachyov I.Yu. (2020) Combination of neutron activation analysis with X-ray fluorescence spectrometry for the determination of rare-earth elements in geological samples. *J Analyt Chem*, vol. 75(7), pp. 878-889. <https://doi.org/10.1134/S106193482007014X>.

24. Koltochnik S.N., Sairanbayev D.S., Chekushina L.V., et al. (2018) Comparison of neutron spectrum in the WWR-K reactor with LEU fuel against HEU one. *NNC RK Bulletin [Vestnik NYATS RK]*, vol. 76(4), pp. 14-17 (in Russian).

25. Hamidatou L., Slamene H., Akhal T., Zouranen B. (2013) Concepts, instrumentation and techniques of neutron activation analysis. In: *Imaging and radioanalytical techniques in interdisciplinary research – fundamentals and cutting edge applications*. Rijeka, Croatia, pp. 141-178. <http://dx.doi.org/10.5772/53686>.

26. Silachyov I. (2020) Elemental analysis of vegetation samples by INAA internal standard method. *J Radioanal Nucl Chem*, vol. 324(1), pp. 97-108. <https://doi.org/10.1007/s10967-020-07051-6>.

27. Nuclear data sub-committee. K0-neutron activation analysis link page (accessed Oct 15, 2021). <http://www.kayzero.com/k0naa/k0naaorg/Links.html>.

28. Rudnick R.L., Gao S. (2014) 4.1 – Composition of the Continental Crust. *Treatise Geochem*, 2d edition, vol. 4, pp. 1-51. <https://doi.org/10.1016/B978-0-08-095975-7.00301-6>.

29. Haynes W.M. (Ed.) (2016) Abundance of elements in the earth's crust and in the sea. CRC handbook of chemistry and physics, 97th edition. Boca Raton, Florida: CRC press, pp. 14-17. ISBN: 9781498754286.

30. Chilian C., St-Pierre J., Kennedy G. (2008) Complete thermal and epithermal neutron self-shielding corrections for NAA using a spreadsheet. *J Radioanal Nucl Chem*, vol. 278(3), pp. 745-749. <https://doi.org/10.1007/s10967-008-1604-8>.

31. Silachyov I.Yu. (2014) Neutron activation analysis of gold in volumetric samples of gold-bearing sulphides using atomic reactor of the INP WWR-K. Proceedings of international conference "Progressive methods of dressing and complex processing of natural and technogenic mineral resources". Plaksinsky readings – 2014. Almaty, Kazakhstan, pp. 155-157 (in Russian).

32. Jodłowski P. (2006) Self-absorption correction in gamma-ray spectrometry of environmental samples – an overview of methods and correction values obtained for the selected geometries. *Nukleonika*, vol. 51(suppl. 2), pp. S21-S25.

33. Hubbell J.H., Seltzer S.M. (accessed Oct 15, 2021) X-ray mass attenuation coefficients. NIST

standard reference database 126. <https://www.nist.gov/pml/x-ray-mass-attenuation-coefficients>.

34. OST 41-08-212-04 (2004) Standart otrasli. Upravlenie kachestvom analiticheskikh rabot. Normy pogreshnosti pri opredelenii himicheskogo sostava mineralnogo syr'ya i klassifikatsiya metodik laboratornogo analiza po tochnosti rezultatov (Industrial standard. Quality management of analytical work. Error guidelines for chemical analysis of mineral resources and precision classification of laboratory analytical techniques). Moscow, VIMS, 23 p. (in Russian).

35. ISO 13528:2015 (2015) Statistical methods for use in proficiency testing by interlaboratory comparisons. Genève, Switzerland, 89 p.

36. Desimoni E., Brunetti B. (2015) About estimating the limit of detection by the

signal to noise approach. *Pharm Anal Acta*, vol. 6, 4 pp. <http://dx.doi.org/10.4172/2153-2435.1000355>.

37. Bode P., Romanò S., Romolo F. (2018) Large sample neutron activation analysis avoids representative sub-sampling and sample preparation difficulties: An added value for forensic analysis. *Forensic Chem*, vol. 7, pp. 81-87. <https://doi.org/10.1016/j.forc.2017.10.002>.

38. Robert F., Poulsen, K.H., Dubé B. (1997) Gold deposits and their geological classification. Proceedings of Exploration 97: Fourth decennial international conference on mineral exploration. Ottawa, Canada, pp. 209-220.

39. Zawisza B., Sito R. (2012) Quantification in X-Ray fluorescence spectrometry. In: X-ray spectroscopy. Rijeka: InTech, pp. 138-162.

© This is an open access article under the (CC)BY-NC license (<https://creativecommons.org/licenses/by-nc/4.0/>). Funded by Al-Farabi KazNU